Contact and friction between catheter and blood vessel

Article *in* Tribology International · February 2007

DOI: 10.1016/j.triboint.2005.10.010

CITATIONS
51

READS
2,617

6 authors, including:

Kazuto Takashima
Kyushu Institute of Technology
113 PUBLICATIONS **463** CITATIONS

SEE PROFILE

Available online at www.sciencedirect.com
ScienceDirect
Tribology International 40 (2007) 319–328
TRIBOLOGY INTERNATIONAL
www.elsevier.com/locate/triboint

Contact and friction between catheter and blood vessel

Kazuto Takashima[a,*], Rei Shimomura[a], Takayuki Kitou[a], Hiroki Terada[a], Kiyoshi Yoshinaka[b], Ken Ikeuchi[a]

[a]*Institute for Frontier Medical Sciences, Kyoto University, 53 Kawahara-cho, Shogoin Sakyo-ku Kyoto 606-8507, Japan*
[b]*National Institute of Advanced Industrial Science and Technology, East, Namiki 1-2-1, Tsukuba 305-8564, Japan*

Received 1 December 2004; accepted 1 October 2005
Available online 29 March 2006

Abstract

Therapeutic vascular catheterization techniques are sometimes hampered by the frictional forces between the blood vessel and the catheter, when contact points of the vessel are changing and deforming during the movement of the catheter. The goal of the present study was to characterize frictional interactions between the blood vessel wall and the catheter using experimental and numerical analysis. First, the frictional force was measured with an experimental apparatus that uses a ball and flattened porcine aorta to simulate frictional forces between the catheter and the vessel. Second, catheter motion was characterized by two-dimensional numerical calculations based on the experimental results. Experimental analysis demonstrated that slip occurred and that friction coefficient between the vessel and the catheter and the deformation of the specimen were small when the contact between the ball and the aorta occurred at a small angle. The compliance of the specimen in the normal direction obtained by the experiment was by far larger than that calculated according to the Hertzian contact theory. Numerical analysis shows that this difference of the parameter of the vessel, which must be determined accurately in surgical simulator, could affect the trajectory of the catheter.

Keywords: Catheter; Friction; Contact condition; Computer simulation; Minimally invasive surgery

1. Introduction

Intravascular catheters have been used for the treatment of various diseases, including acute infarction and aneurysms, but these techniques are sometimes limited by small blood vessel caliber or tortuous vasculature. Further, frictional forces applied by the catheter on the blood vessel wall can induce vasoconstriction and injury and result in reactive intimal proliferation or distal embolization associated with end-organ ischemia and infarction [1]. Therefore, many researches have been carried out to reduce the friction between the catheter and the vessel. For example, lubricants or jelly like materials are often used and a hydrophilic polymer surface has been developed in order to provide lubricity to the catheter [2]. However, much lubricity to the surface of the catheter sometimes results in application of excessive force to the tip of the catheter, leading to perforation of the blood vessel [3].

Various experimental methods can be used to measure frictional forces on the vessel wall, including inclined plane apparatus [2], thrust-collar apparatus [4], pulley apparatus [5], in vitro and in vivo pull-out tests [2,6,7], atomic force microscopy [8,9], and reciprocating friction apparatus [9]. However, these models fail to account for the deformation of the vessel wall in response to these physical forces because the specimens are in contact with each other at the outset, and some of these studies do not use actual blood vessels in their experiments.

On the other hand, computer-based surgical simulator has been developed for medical education, surgical training, surgical planning and intra-operative assistance [10–16]. In these surgical simulators, tissue models that respond in a realistic way are necessary.

Therefore, the goal of the present study was to use experimental and numerical analysis to characterize the frictional forces between the vessel and the catheter, taking into account the angle of approach of the catheter to more appropriately simulate clinical conditions during intravascular catheterization.

*Corresponding author. Tel.: +81 75 751 4840; fax: +81 75 751 4139.
E-mail address: takashima@frontier.kyoto-u.ac.jp (K. Takashima).

0301-679X/$ - see front matter © 2006 Elsevier Ltd. All rights reserved.
doi:10.1016/j.triboint.2005.10.010

Nomenclature

d_n, d_t	normal and parallel displacements of ball in indenter assembly, respectively
E	Young's modulus of blood vessel
F_a	force applied to specimen by universal tester
$\boldsymbol{F}_i$	contact force vector
F_s	force applied to specimen by compressive spring
F_v	shearing force applied to specimen
F_n	normal force applied to specimen
$\boldsymbol{f}_i$	contact force vector of the link i of catheter model from vessel
$\boldsymbol{f}_{ni}$, $\boldsymbol{f}_{ti}$	normal and tangential components of $\boldsymbol{f}_i$ at the contact points, respectively
$\boldsymbol{g}(\boldsymbol{q})$	weight function of catheter model
$\boldsymbol{h}(\dot{\boldsymbol{q}}, \ddot{\boldsymbol{q}})$	centrifugal force (Coriolis force) of catheter model
$\boldsymbol{J}(\boldsymbol{q})$	Jacobian matrix of catheter model
K_c	elastic coefficient of joint of catheter model
K_v	elastic coefficient of vessel deformation
k	spring constant of compressive spring in indenter assembly
L	length of the shaft in indenter assembly
$\boldsymbol{l}_i$	distance between the joint i of catheter model and nearest point of the central curve of vessel model
$\boldsymbol{M}(\boldsymbol{q})$	inertia matrix of catheter model
$\boldsymbol{q}$	joint displacement vector of catheter model
R_c	radius of catheter model
R_v	radius of vessel model
Δt	finite time step for simulation
y	change of vertical position of the lower shaft in indenter assembly
α	slope of specimen
θ	angle of the lower shaft in indenter assembly
μ	friction coefficient between ball and specimen
μ_s	static friction coefficient between ball and specimen
μ_d	dynamic friction coefficient between ball and specimen
τ	sum of elastic force of a mobile joint of catheter model

2. Methods

The experimental protocol consisted of measurement of frictional force using a specialized apparatus (Fig. 1) followed by two-dimensional numerical analysis of the motions of the catheter.

2.1. Experiment

2.1.1. Apparatus

The apparatus simulates a contact between the catheter and the vessel, and consists of a universal tester (MMT-101NB-10, Shimadzu corporation), an indenter assembly and a specimen holder. The indenter assembly was attached to the bottom of the universal tester. A steel ball ($R_a < 0.4\,\mu m$) was attached to the bottom of the shaft, which was supported by ball bearings that allowed the shaft to rotate along the vessel longitudinally. The diameter of the ball was 1 mm because the diameters of the catheter and guidewire are usually 0.3–3.0 and 0.3–1.0 mm, respectively [17]. A potentiometer was attached to the rotation shaft of these ball bearings to change the angle of the lower shaft (θ). A compressive spring corresponding to the bending stiffness of catheter was attached to the shaft. The force applied by the compressive spring (F_s) was equal to zero when the lower shaft turned vertically.

The aorta of matured and healthy pigs (about six months old and 100 kg) were excised immediately postmortem, sectioned longitudinally and flattened on the specimen holder (SUS303; Fig. 2). All soft tissue surrounding the aorta was removed. Three specimens (20×20 mm) were used in each condition. At the center of the each specimen, we fixed a benchmark (10×10 mm, the side is parallel to the vessel axis) by marking with ink. The specimens were clamped at the center point of each side by 3×4 Michel suture clips (10×2 mm) and the benchmarks were extended to 12×12 mm biaxially. This stretching force corresponded to approximately 1 N. As the specimen was clamped only at the sides, the vessel could deform in response to the contact force. The shape and constraint force of the square specimen were different from those of the cylindrical and circumferentially extended vessel found in vivo. Fig. 3 shows the typical histological photomicrographs of the cross-sections of the arteries extended in both conditions. However, as the histological examination of these specimens stained with hematoxylin and eosin (HE) failed to detect the both difference, it is conjectured that the difference of the shape and constrained force of the both specimens does not affect the experimental results. During the experiment, the specimen was immersed in physiological saline solution. Manual stages attached under the bath reservoir were used to adjust the contact points and the slope of the specimen (α). The angle between the porcine aorta and the ball ($\alpha = 5^\circ$, 8°, 12°, 15°, 20° and 25°) was changed. All experiments were performed at room temperature (20–25 °C).

The indenter assembly was descended 1 mm vertically against the porcine aorta at constant speed (1 mm/s) from the contact. The ball contacted the specimen among the benchmarks. The apparatus contained two load cells. The upper load cell was attached to the shaft immediately above the indenter assembly, and the lower load cell was attached to the manual stages of the specimen holder.

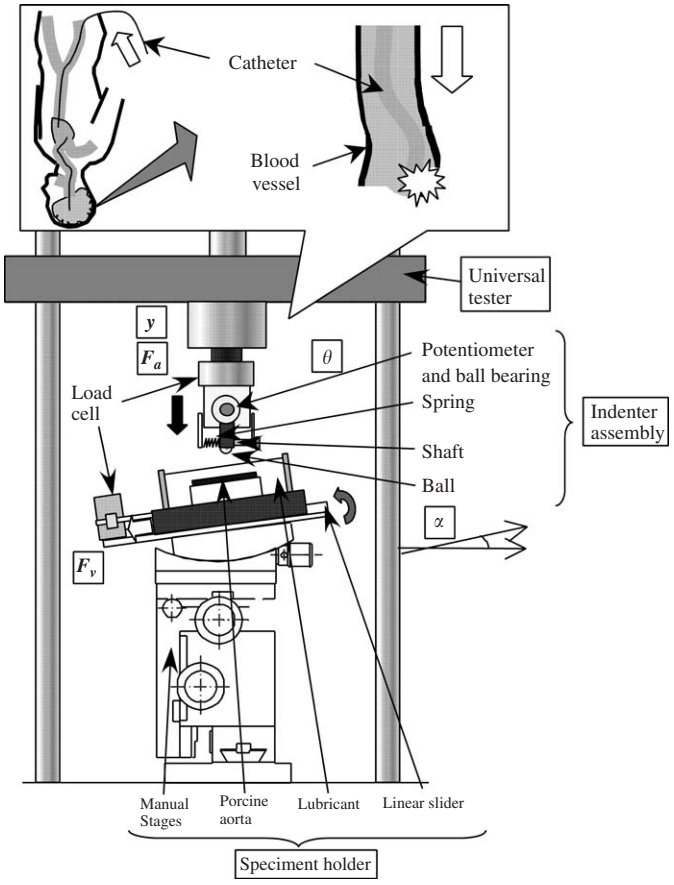

Fig. 1. Schema of friction apparatus.

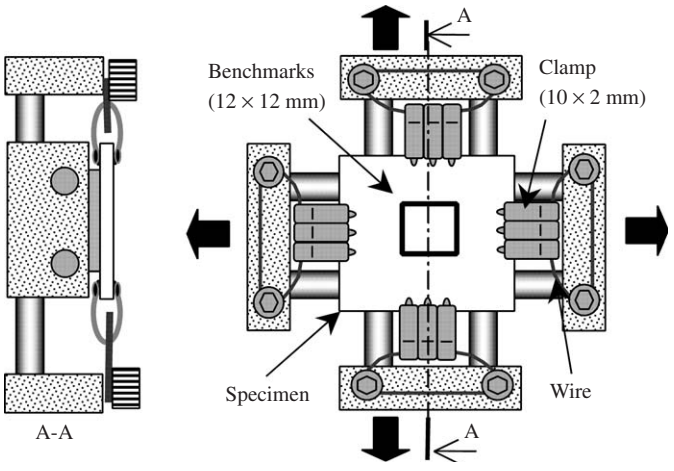

Fig. 2. Specimen holder (setup of specimen hooking).

A linear guide was included between the bath reservoir and the manual stages, and was attached to the lower load cell by an arm. Force applied to the specimen by the universal tester (F_a) was measured by the upper load cell, and the shearing force applied to the specimen (F_v) was measured by the lower load cell. F_v was obtained by subtracting the weight on the linear stage from the force measured by the load cell.

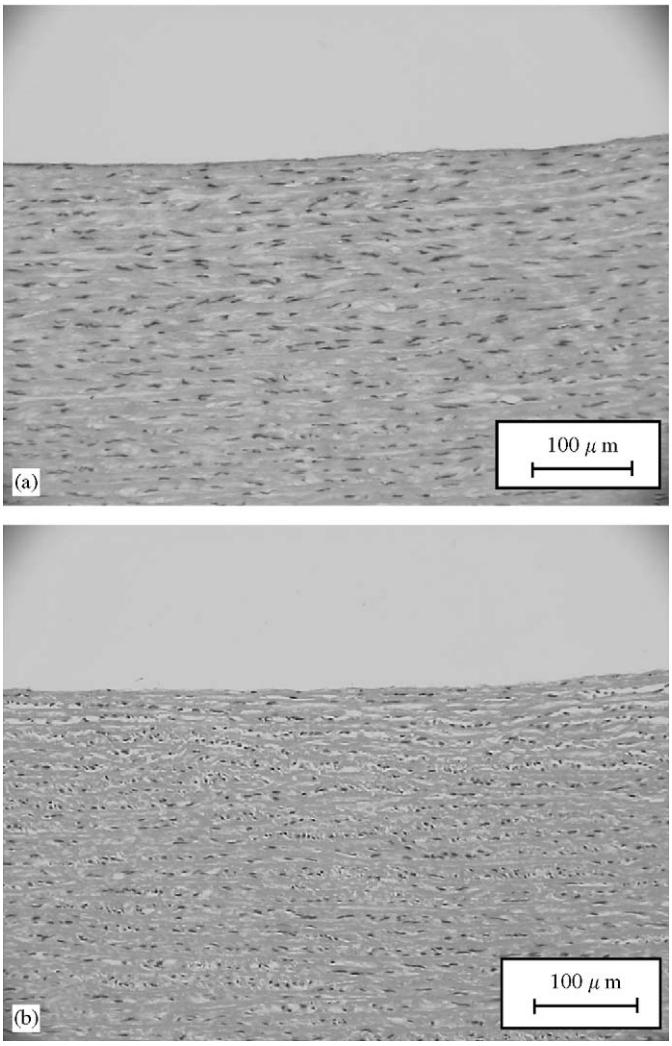

Fig. 3. Representative histological sections stained with hematoxylin and eosin: (a) Biaxially extended specimen. (b) Circumferentially extended specimen.

After the experiment, the aortic tissue was immediately placed in 10% neutral buffered formalin and processed for paraffin embedding, and cross-sections of aorta were prepared and stained with HE to assess the extent of endothelial cell removal from the luminal surfaces. In order to quantitatively evaluate the cell removal, a normalized number of endothelial cells was defined by dividing the number of endothelial cells per 500 μm that were observed in the tested region by the number of cells found in the untested regions. The measurements were performed 10 times for each condition and the results were averaged.

2.1.2. Calculation of friction coefficient and the displacement of the ball

From the experiment, we calculated the friction coefficient and the displacement of the ball. The schema of applied force on the vessel is illustrated in Fig. 4. Because of the deformation of the vessel, these contact forces are distributed over a finite area of contact. The distribution of the contact forces can be substituted with an equivalent

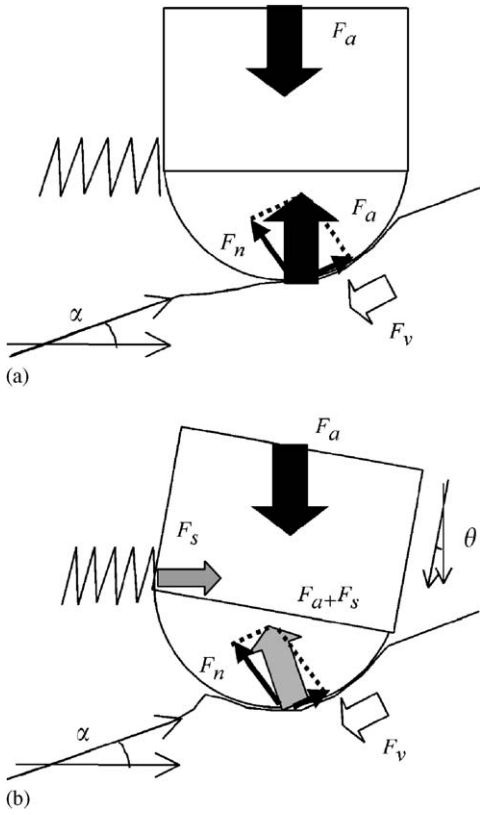

Fig. 4. Geometric parameters for contact without moment: (a) Initial frictional condition. (b) Inclined frictional condition.

force and moment [18]. In this experiment, the moment assumed to be negligible. At the beginning of contact, as the shaft in the indenter assembly turns in the vertical direction, only F_a is applied at the contact point (Fig. 4(a)). If two bodies are rigid and contact at a point, the ball does not slip on the vessel when $\tan\alpha$ is less than the static friction coefficient between the ball and the vessel. In this case, F_v depends on the friction coefficient and F_a. If the ball slips and the shaft leans, the spring attached to the shaft is compressed. Consequently, F_s is also applied (Fig. 4(b)). In both conditions, the normal force applied on the vessel (F_n) and the friction coefficient (μ) are expressed as follows:

$$F_n = F_a \cos\alpha + F_s \sin\alpha, \tag{1}$$

$$F_s = Lk \tan\theta, \tag{2}$$

$$\mu = F_v/(F_a \cos\alpha + F_s \sin\alpha), \tag{3}$$

where L is the length of the shaft and k is the spring constant of the compressive spring. In this study, $L = 47\,\text{mm}$ and $k = 0.034\,\text{N/mm}$. A static friction coefficient (μ_s) and a dynamic friction coefficient (μ_d) were determined as the maximum and mean value of μ during the experiment, respectively. The normal and parallel displacements of the ball (d_n and d_t, respectively) were calculated as follows:

$$d_n = y\cos\alpha - L\{\cos\alpha - \cos(\alpha+\theta)\}, \tag{4}$$

$$d_t = y\sin\alpha + L\{\sin(\alpha+\theta) - \sin\alpha\}, \tag{5}$$

where y is the vertical displacement of the shaft. F_n is expressed as the following equation according to the Hertzian contact theory [19]:

$$F_n = K_v d_n^{3/2}, \tag{6}$$

where K_v is the elastic coefficient of vessel deformation.

2.2. Simulation

2.2.1. Assumptions

The motions of the catheter and the vessel were modeled under the following assumptions [10–11]: (1) the catheter consists of a number of elastic links, with each joint rotating with one degree of freedom, and all links moves in a plane during simulation, and (2) the vessel is an elastic circular cylinder (Fig. 5). The force was computed considering the contact between the catheter and the vessel.

2.2.2. Catheter model

The catheter consists of a number of elastic links. Multiple links can be expressed using Newton–Euler equations of motion as follows [10,11]:

$$\boldsymbol{M}(\boldsymbol{q})\ddot{\boldsymbol{q}} = \tau - \boldsymbol{\tau}_N, \tag{7}$$

$$\tau_N = \boldsymbol{h}(\dot{\boldsymbol{q}}, \ddot{\boldsymbol{q}}) + \boldsymbol{g}(\boldsymbol{q}), \tag{8}$$

$$\tau = \sum_i^n \boldsymbol{J}_r^T(q)\boldsymbol{F}_i - K_c\left[\boldsymbol{q} - \boldsymbol{q}_0\right], \tag{9}$$

where $\boldsymbol{q}$ is the joint displacement vector, $\boldsymbol{M}(\boldsymbol{q})$ means the inertia matrix, $\boldsymbol{h}(\dot{\boldsymbol{q}}, \ddot{\boldsymbol{q}})$ means centrifugal force (Coriolis force), $\boldsymbol{g}(\boldsymbol{q})$ means weight function, $\boldsymbol{\tau}$ is defined as the sum of elastic force (an elastic coefficient K_c) of a mobile joint. $\boldsymbol{J}(\boldsymbol{q})$ is Jacobian matrix, and $\boldsymbol{F}_i$ is the contact force vector. However, $\boldsymbol{g}(\boldsymbol{q})$ is assumed to be $\boldsymbol{0}$ in this study.

The parameters used in this study are summarized in Table 1. K_c was estimated from the mechanical property of a commercial guidewire. Further, the proximal portion of the catheter was assumed to move at a constant speed (1 mm/s).

2.2.3. Vessel model

The shape of the vessel was defined by the centerline and the radii (R_v). The centerlines that determine the shape of the whole vessel are represented by equations shown in Fig. 6. In these models, the catheter was inserted from the origin along x-axis. In this simulation, $R_v = 0.5\,\text{mm}$.

Deformation of the vessel tube in the radial direction is modeled with an elastic coefficient (K_v), and the friction against the vessel wall is modeled with μ_s and μ_d.

To determine whether there is contact between the catheter and the vessel, the distances between the catheter model joints and the centerline of the vessel were calculated. The geometry of the contact point can be estimated for comparison with R_v and R_c. In the case of contact, the contact force vector of the link i from the

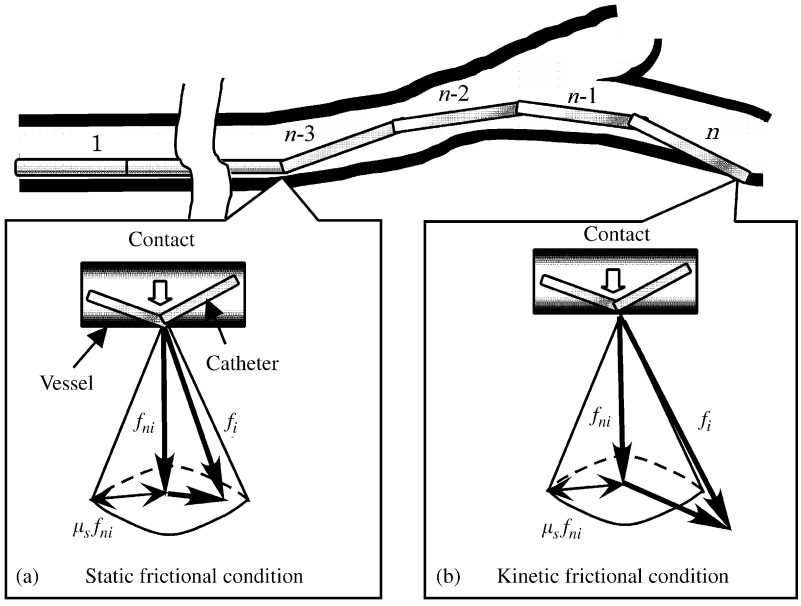

Fig. 5. Catheter model with elastic joints.

Table 1
Prameters of catheter model used in the simulation

Radius (mm)	0.5
Density (kg/m^3)	6.5×10^6
Number of links	20
Link length (mm)	0.1
K_c (N mm/rad)	8.9

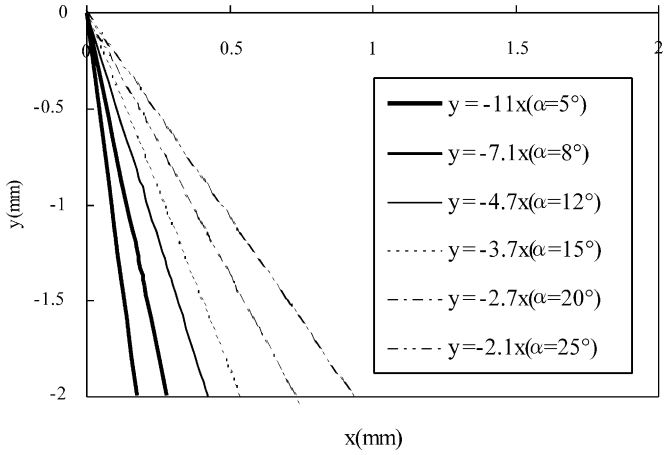

Fig. 6. Center line of vessel model for different angle (α).

vessel ($\boldsymbol{f}_i$) was considered. Next, $\boldsymbol{f}_i$ was divided into the normal and tangential components ($\boldsymbol{f}_{ni}$ and $\boldsymbol{f}_{ti}$, respectively) of the vessel at the contact points to examine the frictional condition. Similarly to Eq. (6) based on Hertzian contact theory [19], $\boldsymbol{f}_{ni}$ is expressed as follows:

$$\boldsymbol{f}_{ni} = \boldsymbol{K}_v(||\boldsymbol{l}_i|| + R_c - R_v)^{3/2}\frac{\boldsymbol{l}_i}{\|\boldsymbol{l}_i\|}, \tag{10}$$

Table 2
Parameters of blood vessel model used in the simulation

Test name	K_v (N/mm$^{3/2}$)	μ_s	μ_d
TT	0.5	0.08	0.04
TE	0.5	$-0.0047\theta + 0.144$	$-0.0034\theta + 0.094$
ET	32	0.08	0.04
EE	32	$-0.0047\theta + 0.144$	$-0.0034\theta + 0.094$

where $\boldsymbol{l}_i$ is the distance between the joint i and nearest point of the central curve. This equation is possible if $||\boldsymbol{l}_i|| + R_c \cong R_v$. In this study, the position of centerline of the vessel was assumed to be constant.

Next, based on the work by Ikuta et al. [10,11], $\boldsymbol{F}_i$ was calculated in the static and kinetic conditions (refer to appendix). A frictional cone (Fig. 5) was used to express the effect of friction with movement along smooth contact surfaces, and the difference between the static and kinetic frictional conditions.

2.2.4. Calculation of parameters of blood vessel for simulation

The parameters used in the simulation are summarized in Table 2. We calculated for four cases and the test names were TT, TE, ET and EE. K_v and μ were determined by two different methods. The first and second letters of the test names show the methods to obtain K_v and μ, respectively.

"T" of the test name stands for "theoretical". Namely, we first estimated K_v and μ from the previous researches [9,20]. Substituting Young's modulus of the blood vessel ($E = 4 \times 10^{-1}$ MPa) [20] into the following equation based on the Hertzian contact theory [19], $K_v = 0.5$ N/mm$^{3/2}$:

$$K_v = 16\sqrt{R_c}E/9. \tag{11}$$

In the derivation of this value, it is assumed that Poisson ratio is 0.5 as Carew reported that the blood vessel wall is approximately incompressible [21].

"E" of the test name stands for "experimental". Secondly, we determined K_v and μ using the experimental results in this study (refer to Section 3.1.2). The friction coefficients were assumed to be functions of the contact angle between the catheter and the vessel.

Using these parameters, the positions in each condition at 0.4 s from the contact were calculated.

2.2.5. Calculation algorithm

We calculated Eq. (7) using the contact force as shown in Section 2.2.3 at every finite time step Δt as follows:

$$\ddot{\boldsymbol{q}} = \boldsymbol{M}^{-1}(\boldsymbol{q})[\boldsymbol{\tau} - \boldsymbol{h}(\dot{\boldsymbol{q}}, \ddot{\boldsymbol{q}}) - \boldsymbol{g}(\boldsymbol{q})], \tag{12}$$

$$\dot{\boldsymbol{q}}(t + \Delta t) = \dot{\boldsymbol{q}}(t) + \ddot{\boldsymbol{q}}(t)\Delta t, \tag{13}$$

$$\ddot{\boldsymbol{q}}(t + \Delta t) = \boldsymbol{q}(t) + \dot{\boldsymbol{q}}(t)\Delta t + (\Delta t)^2\ddot{\boldsymbol{q}}(t)/2. \tag{14}$$

3. Results

3.1. Experiment

3.1.1. Effect of contact angle and contact velocity

The results of experiments are shown in Figs. 7–12. Example of the transition of F_v is shown in Fig. 7. F_v was dependent on the initial angles (α). Figs. 8 and 9 show the relationship between α and the friction coefficient (μ_s and μ_d, respectively). When $\alpha > 15^\circ$, μ_s and μ_d are small (< 0.017). μ_s have a maximum (0.13) at 12° and minimum (0.015) at 20°. μ_d also shows similar dependence on α, whereas the values are different. The mean values of μ_d is 0.046.

Figs. 10 and 11 show the relationship between α and the displacements (d_n and d_t, respectively). In Figs. 10 and 11, the vertical axis shows the maximum displacement of the ball until the shaft moves for 0.2 mm vertically. When α increased, d_n remained nearly constant (approximately 0.38 mm), and d_t increased. d_t have a maximum (0.36 mm) at 20°.

The histological photographs observed no lesions of the intima of the blood vessels. Fig. 12 shows the relationship between α and normalized number of endothelial cells. The normalized number of endothelial cells remained nearly constant (approximately 0.80). Namely, the numbers of endothelial cells were almost unchanged.

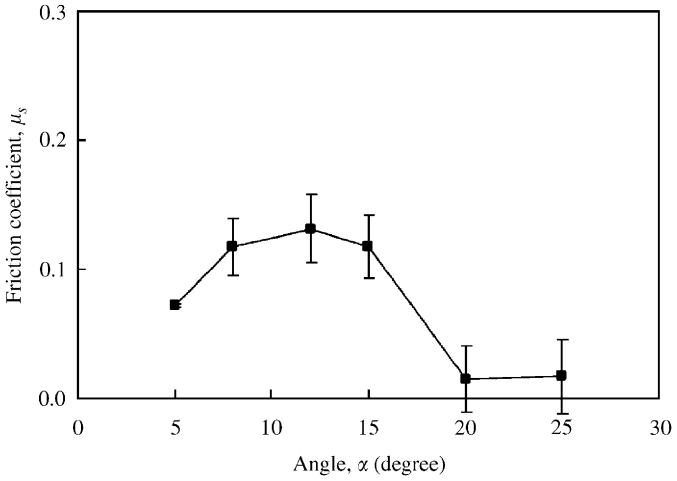

Fig. 8. Initial angle (α) vs. friction coefficient (μ) (maximum value).

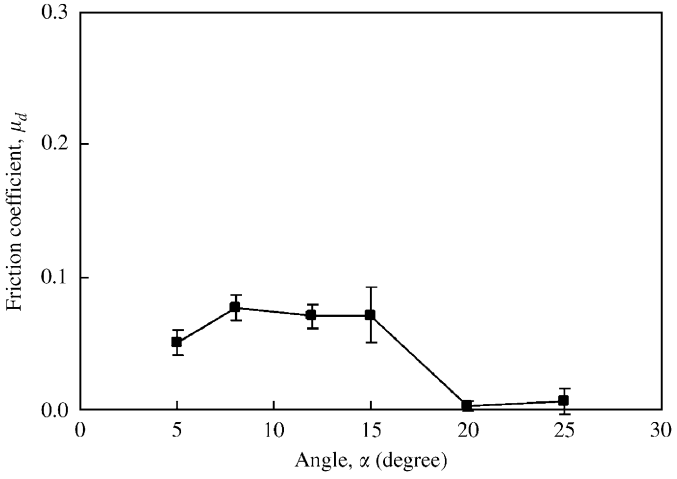

Fig. 9. Initial angle (α) vs. friction coefficient (μ) (mean value).

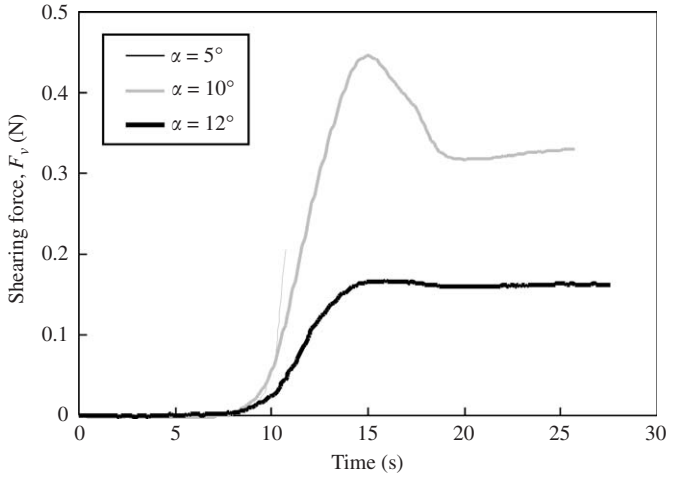

Fig. 7. Example of the transition of shearing force applied on the specimen (F_v).

3.1.2. Calculated vessel parameters for simulation

The relationship between d_n and F_n is shown in Fig. 13. By curve fitting with Eq. (6), $K_v = 32\,\mathrm{N/mm^{3/2}}$. The solid line in Fig. 13 shows the curve fitted with Eq. (6). μ_s and μ_d were assumed to express the following equations by linear

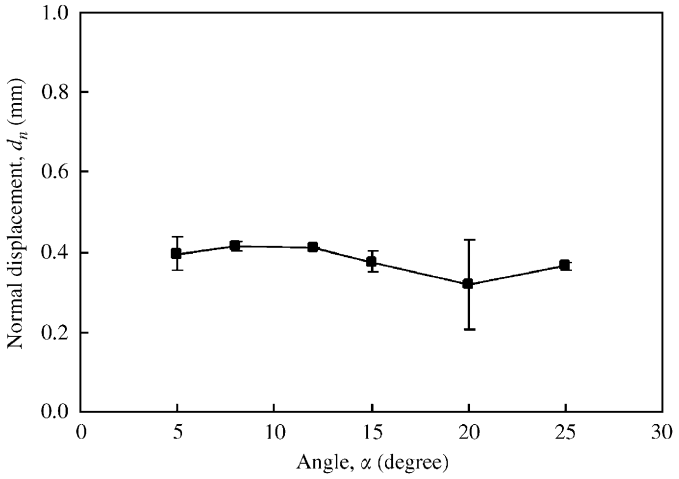

Fig. 10. Initial angle (α) vs. normal displacement (d_n).

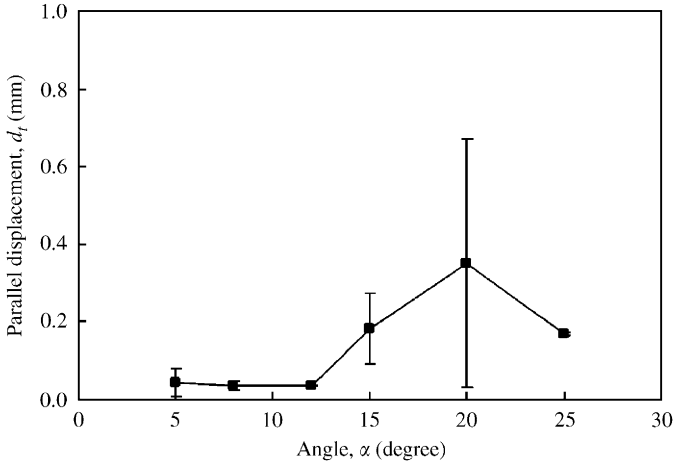

Fig. 11. Initial angle (α) vs. parallel displacement (d_t).

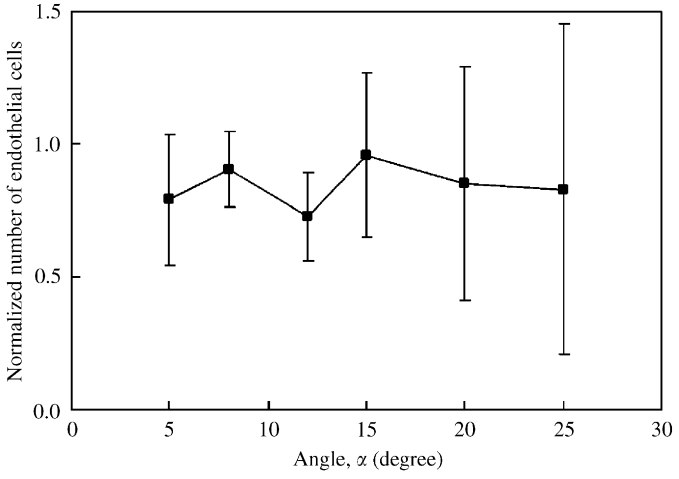

Fig. 12. Initial angle (α) vs. number of endothelial cells.

curve fitting of Figs. 8 and 9:

$$\mu_s = -0.0047\theta + 0.144, \quad (15)$$

$$\mu_d = -0.0034\theta + 0.094. \quad (16)$$

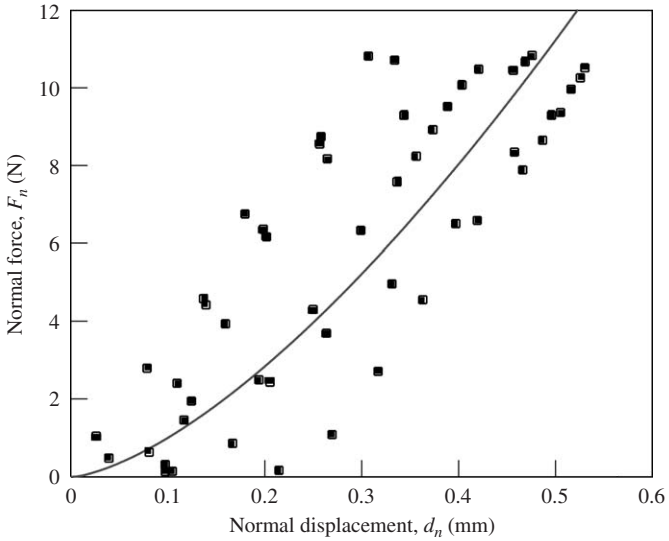

Fig. 13. Normal displacement (d_n) vs. normal force (F_n).

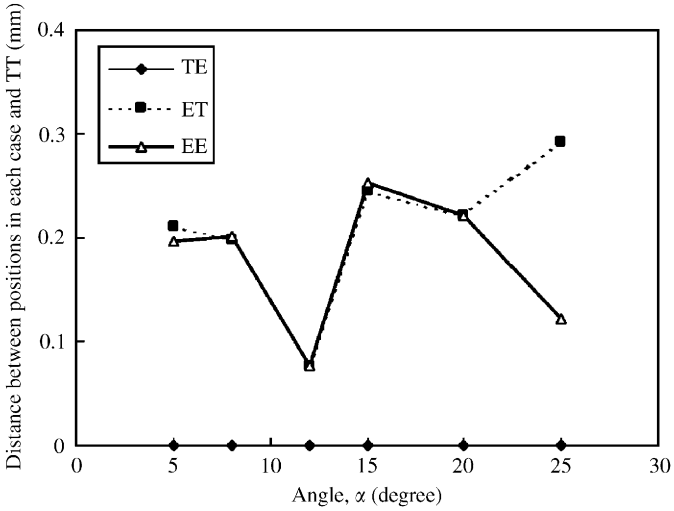

Fig. 14. Variation of distance between positions in each case and TT with respect to the angle (α) of the porcine aorta and the ball obtained by simulation. Descriptions explaining TT, TE, ET and EE are shown in Table 2.

Consequently, the parameters shown in Table 2 were obtained.

3.2. Simulation

The variation of distance between the theoretical point with respect to the α of the porcine aorta and the ball is illustrated in Fig. 14. The vertical axis is the distance between positions in each case. When K_v was changed (in ET, EE), the variation of distance was large (more than 0.076 mm). When only μ was changed (in TE), the variation of distance was very small (less than 0.00043 mm).

4. Discussion

4.1. Effect of contact angle on the parameter of blood vessel

In this experiment, parallel displacement of the ball occurred even when $\alpha = 5^\circ$, and displacement increased with further increases in α. Similarly, the friction coefficient changed according to α, while the mean value of μ_d (0.046) was in good agreement with that in the previous study (0.04) [9]. In preliminary experiments measured in an inclined plane apparatus (Fig. 15), the slip started when $\alpha = 16^\circ$. Based on these results, the cause of parallel displacements may be different when comparing small and large angle conditions. For example, when α is small, the parallel displacement occurred secondary to deformation of the vessel. By contrast, when α was greater than 16° and the tangential component of F_a was large, slip occurred, and the parallel displacement was relatively large. Consequently, the slip decreased the friction coefficient. As shown in Fig. 10, the normal displacement presents almost constant value in all conditions. This result indicates that the mechanical properties of vessel has more effect on the normal displacement than the slip.

The previous study using a reciprocating friction apparatus [9] documented cell removal (normalized numbers of endothelial cells were 0.53–0.61), while no intimal lesions were observed after our experiments. However, in this previous study, the total sliding distance was more than 250 mm, while the parallel displacement was less than 0.35 mm in our experiment (Fig. 11). It seems that cell removal needs higher stress or longer sliding distance.

4.2. Effect of the parameter of blood vessel on surgical simulator

When K_v was changed (in ET, EE), the variation of trajectory of catheter was large as shown in Fig. 14. On the other hand, when only μ was changed (in TE), the variation was very small. Namely, K_v has more effect than μ_s and μ_d on the trajectory of the tip of catheter. The difference can be attributed to the large differences between these values. K_v obtained by the experiment was 65 times larger than that calculated according to the Hertzian contact theory, while μ obtained by the experiment was 0.053–1.9 times larger than that of the previous study. Moreover, K_v can affect μ through F_n, as shown in Eqs. (1), (3) and (6).

As K_v differs depending on the calculation methods, the compliance in the normal direction cannot be expressed according to the Hertzian contact theory. Moreover, the variances in vessel stiffness based on the biological milieu should be considered.

These data may assist in the construction of a device that enables simulation of patient-specific vascular beds that could be used as a pre-treatment planning tool. Such a simulator could help determine the proper choice of catheter (e.g., preferable bending angle, bending stiffness of the guidewire) and planning of interventional procedure. For the accuracy of these simulators, it is important to determine these parameters accurately taking the vessel deformation into the consideration.

Further, intraoperative fluoroscopic catheter data could be used to modify this simulation apparatus to provide real-time problem solving abilities in the context of complex vascular anatomy or problematic vascular lesions. A complete characterization of contact-related phenomena would involve complex continuum mechanics relationships whose computation is difficult in real time. Actually, as the vessel deforms according to the contact, the contact occurs between two real (non-rigid, possibly inelastic) bodies mutually transmitting a distribution of contact forces over a finite area of contact. Besides that, moment can occur and the contact point can move gradually. However, by using Eq. (10), which is relatively simple and approximates physiologic conditions using a specialized apparatus, real-time processing is possible.

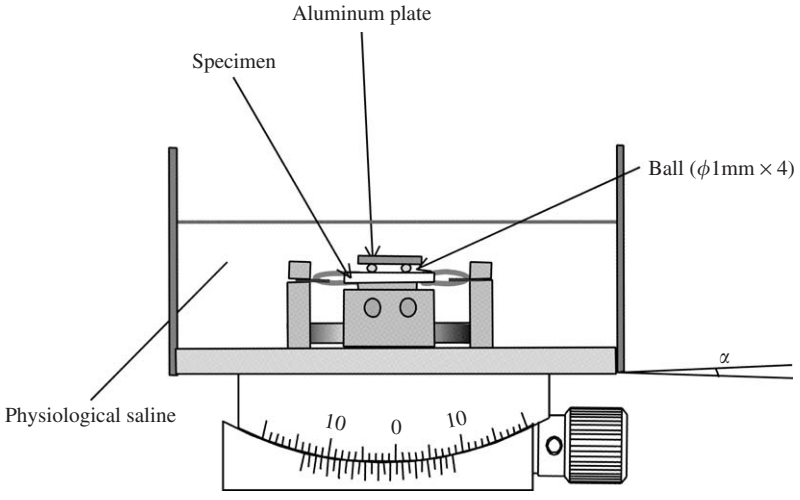

Fig. 15. Inclined plane apparatus; four balls are attached to each vertex of an aluminum square plate and placed on the specimen.

4.3. Future works

Several problems need to be addressed before this model could be practically applied:

1. Analysis must be expanded to 3-dimensions and including torsional forces exerted by the catheter.
2. Other physiologic parameters must be integrated into the model. For example:
   - Contact speed.
   - The material, the radius and bending stiffness of catheter may affect the stress concentration of the contact surface.
   - Constraint force of vessel (e.g. radial and longitudinal tension) and tangential forces affect the shearing force between the contact points.
   - The lubricating effect of plasma [5] can reduce frictional forces.
   - Intimal lesions can affect frictional forces.
   - The effect of moment was ignored in this study.

Measurement of these parameters in vivo with a new tactile sensor system [22] may allow integration of these variables in the simulator system and allow for better development of catheter actuators to improve manipulation ability [23].

5. Conclusions

In this study, we investigated the frictional interactions between the blood vessel and the catheter. When the catheter contacted the blood vessel at a small angle ($<75^\circ$), friction coefficient between the vessel and the catheter was small (<0.017) and moreover the deformation of the blood vessel was also small. The compliance of the vessel in the normal direction obtained by the experiment was 65 times larger than that calculated according to the Hertzian contact theory. This difference of the parameter of the vessel, which must be determined accurately in surgical simulator, could affect the trajectory of the catheter. The results of this study would be useful to determine the parameters for the surgical simulator.

Acknowledgment

This paper was supported in part by Center of Excellence for Research and Education on Complex Functional Mechanical Systems (COE program of the Ministry of Education, Culture, Sports, Science and Technology, Japan).

Appendix A

Based on the work by Ikuta et al. [10–11], $\boldsymbol{F}_i$ is calculated in the static and kinetic conditions as follows. In this model, $\boldsymbol{f}_i$ is expressed as follows:

$$\boldsymbol{f}_i = (\|\boldsymbol{f}_{ni}\| / \cos\beta)\,\frac{\boldsymbol{v}_i}{\|\boldsymbol{v}_i\|} \tag{A.1}$$

where β is the angle between $\boldsymbol{f}_i$ and $\boldsymbol{f}_{ni}$ and $\boldsymbol{v}_i$ is the velocity vector of the joints. $\boldsymbol{f}_{ti}$ is obtained by

$$\boldsymbol{f}_{ti} = \boldsymbol{f}_i - \boldsymbol{f}_{ni} \tag{A.2}$$

From these vectors, the frictional condition can be judged. If

$$||\boldsymbol{f}_{ti}|| \leqslant ||\mu_s||\boldsymbol{f}_{ni}|| \tag{A.3}$$

then it becomes the static frictional condition and the reaction force $\boldsymbol{F}_i$ is expressed as follows:

$$\boldsymbol{F}_i = \boldsymbol{f}_i. \tag{A.4}$$

If

$$||\boldsymbol{f}_{ti}|| > \mu_s||\boldsymbol{f}_{ni}||. \tag{A.5}$$

then it becomes kinetic frictional condition and $\boldsymbol{F}_i$ is expressed as follows:

$$\boldsymbol{F}_i = \mu_d\|\boldsymbol{f}_{ni}\|\,\frac{\boldsymbol{f}_{ti}}{\|\boldsymbol{f}_{ti}\|} + \boldsymbol{f}_{ni} \tag{A.6}$$

References

[1] Capron L, Bruneval P. Influence of applied stress on mitonic response of arteries to injury with a balloon catheter: quantitative study in rate thoracic aorta. Cardiovasc Res 1989;23:941–8.
[2] Nagaoka S, Akashi R. Low-friction hydrophilic surface for medical devices. Biomaterials 1990;11:419–24.
[3] Mitsudou K. PTCA technique. Igaku shoin, 1999 [in Japanese].
[4] Ikeuchi K, Tadaoki, Norikane H, et al. Water lubrication of polyurethane grafted with dimethylacrylamide for medical use. Wear 1993;161:179–85.
[5] Triolo PM, Andrade JD. Surface modification and characterization of some commonly used catheter materials. II. Friction characterization. J Biomed Mater Res 1983;17:149–65.
[6] Uyama Y, Tadokoro H, Ikada Y. Low-frictional catheter materials by photo-induced graft polymerization. Biomaterials 1991;12:71–5.
[7] Marmieri G, Pettenati M, Cassinelli C, Morra M. Evaluation of slipperiness of catheter surfaces. J Biomed Mater Res 1996;33:29–33.
[8] Nurdin N, Weilandt E, Textor M, Taborelli M, Spencer ND, Descouts P. Reduced frictional resistance of polyurethane catheter by means of a surface coating procedure. J Appl Polym Sci 1996;61:1939–48.
[9] Caldwell RA, Woodell JE, Ho SP, Shalaby SW, Boland T, Langan EM, et al. In vitro evaluation of phosphonylated low-density polyethylene for vascular applications. J Biomed Mater Res 2002;62(4):514–24 [December 5].
[10] Ikuta K, Takeichi M, Namiki T. Virtual Endoscope System with Force Sensation. In: Proceedings of the IEEE International Conference on Robotics and Automation ICRA99, p. 1715–21.
[11] Ikuta K, Iritani K, Fukuyama J, Takeichi M. Portable virtual endoscope system with force and visual display. In: Proceedings of the IEEE/RSI International Conference on Intelligent Robots and Systems, vol. 1. 2000. p. 720–6.
[12] Suzuki S, Suzuki N, Hattori A, Uchiyama A. Development of virtual surgery simulation system with the sphere-filled organ model, the transactions of the Institute of Electronics, Information and Communication Engineers. D-2 2003;J86-D-II(9):1341–9 [in Japanese].
[13] Martin RW, Johnson CC. Design characteristics for intravascular ultrasonic catheters. Int J Card Imaging 1989;4(2–4):201–16.

[14] Cotin S, Delingette H, Bro-Nielsen M, Ayache N, Clement JM, Tassetti V, et al. Geometric and physical representations for a simulator of hepatic surgery. Stud Health Technol Inform 1996;29:139–51.
[15] Wang Y, Chui C, Lim H, Cai Y, Mak K. Real-time interactive simulator for percutaneous coronary revascularization procedures. Comput Aided Surg 1998;3(5):211–27.
[16] Berkley J, Weghorst S, Gladstone H, Raugi G, Berg D, Ganter M. Fast finite element modeling for surgical simulation. Stud Health Technol Inform 1999;62:55–61.
[17] Haga Y, Esashi M. Medical devices for minimally invasive diagnosis and treatment using micro-nano machining. J JSAEM 2004;12(2):106 [in Japanese].
[18] Bicchi A, Salisbury JK, Brock DL. Contact sensing from force measurements. Int J Robotics Res 1993;12(3):249–62.
[19] Timoshenko SP, Goodier JN. Theory of elasticity. New York: McGraw-Hill.
[20] Bergel DH. Static elastic properties of the arterial wall. J Physiol 1961;156:445–57.
[21] Carew TE, Vaishnav RN, Patel DJ. Compressibility of the arterial wall. Circ Res 1968;23:61–8.
[22] Takashima K, Yoshinaka K, Okazaki T, Ikeuchi K. An endoscopic tactile sensor for low invasive surgery. Sensors Actuators A: Physical 2005;119(2):372–83.
[23] Lim G, Park K, Sugihara M, Minami K, Esashi M. Future of active catheters. Sensors Actuators A: Physical 1996;56(1–2):113–21.